Acta Cryst. (1996). D52, 435–446

Structure of Human Salivary α-Amylase at 1.6 Å Resolution: Implications for Its Role in the Oral Cavity

NARAYANAN RAMASUBBU,[a]* VENUGOPALAN PALOTH,[a] YAOGUANG LUO,[b] GARY D. BRAYER[b] AND MICHAEL J. LEVINE[a]

[a]*Department of Oral Biology and Dental Research Institute, School of Dental Medicine, State University of New York at Buffalo, Buffalo, NY 14214, and* [b]*Department of Biochemistry and Molecular Biology, University of British Columbia, Vancouver, British Columbia, Canada V6T 1Z3. E-mail: subbu@crystal1.sdm.buffalo.edu*

(Received 25 May 1995; accepted 10 October 1995)

Abstract

Salivary α-amylase, a major component of human saliva, plays a role in the initial digestion of starch and may be involved in the colonization of bacteria involved in early dental plaque formation. The three-dimensional atomic structure of salivary amylase has been determined to understand the structure–function relationships of this enzyme. This structure was refined to an *R* value of 18.4% with 496 amino-acid residues, one calcium ion, one chloride ion and 170 water molecules. Salivary amylase folds into a multidomain structure consisting of three domains, *A*, *B* and *C*. Domain *A* has a $(\beta/\alpha)_8$-barrel structure, domain *B* has no definite topology and domain *C* has a Greek-key barrel structure. The Ca^{2+} ion is bound to Asn100, Arg158, Asp167, His201 and three water molecules. The Cl^- ion is bound to Arg195, Asn298 and Arg337 and one water molecule. The highly mobile glycine-rich loop 304–310 may act as a gateway for substrate binding and be involved in a 'trap-release' mechanism in the hydrolysis of substrates. Strategic placement of calcium and chloride ions, as well as histidine and tryptophan residues may play a role in differentiating between the glycone and aglycone ends of the polysaccharide substrates. Salivary amylase also possesses a suitable site for binding to enamel surfaces and provides potential sites for the binding of bacterial adhesins.

1. Introduction

α-Amylases (E.C. 3.2.1.1) catalyze the hydrolysis of α-1,4-glucosidic linkages in starch and other related polysaccharides. These enzymes are ubiquitous in both the plant and animal kingdoms. In humans, amylase is present in both salivary and pancreatic secretions and is produced by two different loci, *AMY1* and *AMY2*, respectively. Considerable sequence similarity exists between the salivary enzyme and α-amylases from other sources, especially human and porcine pancreas. Amylases are monomeric calcium-binding proteins with a single polypeptide chain folded into three domains, and belong to the family of proteins that harbor the $(\beta/\alpha)_8$-barrel topology first identified in the triose phosphate isomerase (Banner *et al.*, 1975; Alber *et al.*, 1981; Farber & Petsko, 1990). The active site for the enzymes of this family is generally located at the C-terminal end of the central β-barrel. Unlike triose phosphate isomerase, α-amylases have two additional domains of approximately 70–100 amino acids in size. The first of these domains is formed between the third β-strand and the third helix of the central barrel structure. The calcium ion is generally located in this domain (Matsuura, Kusunoki, Harada & Kakudo, 1984; Buisson, Duee, Haser & Payan, 1987; Klein & Schulz, 1991; Larson, Greenwood, Cascio, Day & McPherson, 1994). The second domain is a β-only structure and generally adopts a Greek-key topology.

Amylase is the most abundant enzyme in human saliva and is comprised of two major families (family A which is glycosylated and family B which is non-glycosylated) with several isoenzymes in each family. The secreted enzyme, blocked by a pyroglutamic acid residue at the N-terminus, consists of 496 amino acids with a molecular weight of ~56 000. The complete amino-acid sequence for human salivary amylase has been deduced from the cDNA sequence (Nishide, Emi, Nakamura & Matsubara, 1986). Salivary amylase is a multifunctional enzyme involved with at least three distinct biological functions. First, the hydrolytic activity is responsible for the initial breakdown of the polymeric starch to short oligomers. Second, amylase in solution binds with high affinity to viridans oral streptococci, a function that may lead to the clearance and/or adherence of these bacteria in the oral cavity. Interestingly, amylase bound to the bacterial surface retains approximately 50% of its enzymatic activity (Scannapieco, Bergey, Reddy & Levine, 1989; Scannapieco, Bhandary, Ramasubbu & Levine, 1990; Douglas, 1990; Douglas, Heath & Gwynn, 1992). Thus, bacteria-bound amylase is capable of hydrolyzing starch to glucose, which can be used as a food source and then metabolized to lactic acid. Localized acid production by bacteria can lead to the dissolution of tooth enamel, a critical step in dental caries progression. Third, several lines of evidence indicate that salivary amylase bound to tooth enamel or hydroxyapatite may

© 1996 International Union of Crystallography
Printed in Great Britain – all rights reserved

play a role in dental plaque formation: (1) α-amylase is a constituent of the acquired enamel pellicle (Örstavik & Kraus, 1973; Al-Hashimi & Levine, 1989) in which amylase may act as a receptor for bacterial adhesion to the tooth surface; (2) amylase has been identified in the dental plaque (Birkhed & Skude, 1978; DiPaola, Herrera & Mandel, 1984); and (3) the amylase bound to hydroxyapatite interacts with several species of oral streptococci which are among the first inhabitants of dental plaque (Scannapieco, Torres & Levine, 1996). Taken together, these multiple functions of amylase suggest it may play a significant role in dental plaque formation and in the subsequent process of dental caries formation and progression.

As a result of its role in the oral microbial ecology, we have initiated studies directed towards gaining a detailed understanding of the structural requirements necessary for the bacteria-binding characteristics of salivary amylase. Although three-dimensional structures of fungal as well as mammalian amylases have been described (Matsuura *et al.*, 1984; Buisson *et al.*, 1987; Boel *et al.*, 1990; Brady, Brozozowski, Derewenda, Dodson & Dodson, 1991; Swift *et al.*, 1991; Qian, Haser & Payan, 1993; Larson *et al.*, 1994; Kadziola, Abe, Svensson & Haser, 1994; Brayer, Luo & Withers, 1996), human salivary amylase exhibits the highest bacterial binding activity to oral bacteria (Douglas, Pease & Whiley, 1990). Therefore, the structure determination and complementary mutational studies are necessary to gain a better understanding of α-amylase functions and in the attempts to manipulate the biological activities of salivary α-amylase. In this report, we describe the structure of salivary amylase as determined by X-ray diffraction methods and refined to a resolution of 1.6 Å and discuss the potential implications of this structure on biological activity.

2. Materials and methods

Non-glycosylated salivary α-amylase isoenzyme B1 was purified from human parotid saliva as previously described (Scannapieco *et al.*, 1989). Crystals suitable for X-ray analysis were obtained using a protein concentration of 20–30 mg ml^{-1} in 10 m*M* Tris–HCl containing 5 m*M* $CaCl_2$, pH 9.0 (Ramasubbu, Bhandary, Scannapieco & Levine, 1991). The crystals were mounted in Lindemann capillaries. Initial diffraction data were collected using an Enraf–Nonius FAST area detector system and processed using the *MADNES* suite of programs (Ramasubbu *et al.*, 1991). A complete data set (92% to 3.0 Å) was used in the early trials for the structure solution. A second data set was collected on an R-AXIS II imaging-plate detector. The X-ray source was a Rigaku RU-200 rotating-anode generator operating at 50 kV and 100 mA with the crystal-to-detector distance set at 60.1 mm. 100 frames were measured covering a total of 100° with the rotation axis oriented about 6° to the *a* axis along with an additional 60 frames in a second orientation about 45° to the first one to give a data set which is 93% complete to 1.6 Å. Processing was carried out using the standard *R-AXIS* program package. A total of 181 285 reflections were collected of which 68 570 reflections were unique with an $R_{\rm merge} = 7.2\%$. Crystals of α-amylase are orthorhombic and of space group $P2_12_12_1$ with unit-cell dimensions of $a = 53.16$, $b = 75.39$ and $c = 136.60$ Å. The new *c* parameter refined to a value which is approximately 1.3% less than the value obtained previously (Ramasubbu *et al.*, 1991).

Initial attempts to solve the structure by molecular replacement (MR) using the atomic coordinates for TAKA amylase (Matsuura *et al.*, 1984) deposited in the Protein Data Bank (entry 2TAA) as a search model were unsuccessful. Rotation-function calculations were carried out using the programs *X-PLOR* (Brünger, 1988) or *MERLOT* (Fitzgerald, 1988). For these trials, data collected using the FAST system were employed. Numerous attempts using all three domains, only *A/B* domains or only the *A* domain with and without side chains were not successful. The application of Patterson-correlation refinement (Brünger, 1990) for the rotation-function solutions also did not improve the quality of the results. At this stage, the use of human pancreatic amylase coordinates (Brayer *et al.*, 1996) in the MR procedures led to a unique solution in both rotation as well as translation-function procedures using *X-PLOR*. Although, the first data set collected on the FAST system also gave rise to a unique solution in both rotation and the translation-function procedures using *X-PLOR* (Brünger, 1988), further analysis was performed using the second data set. No attempt was made to merge the two data sets.

To begin structural refinement the pancreatic amylase coordinates were rotated and translated according to the values obtained in the MR calculations. This model was then subjected to a rigid-body refinement using *X-PLOR* with the polypeptide chain segments 1–99 + 169–404, 100–168, and 405–496 treated as individual rigid-body segments. These correspond to domains *A*, *B* and *C*, respectively. An initial *R* factor of 39% for data in the range 8.0–2.5 Å was obtained. In this analysis amino acids which differed from the human pancreatic model (Table 1) were mutated to alanine unless a glycine was present in the salivary amylase sequence (residue 171). At this point energy minimization was carried out followed by simulated annealing (SA) using a temperature gradient of 3000–300 K in increments of 25 K and a time step of 0.5 fs as implemented in *X-PLOR*. The second stage of refinement consisted of 100 cycles of positional refinement followed by ten cycles of individual *B*-factor refinement which reduced the *R* factor to 21%. All salivary amylase residues not included to this point were added and manually fitted to $[F_o - F_c]$ and $[2F_o - F_c]$ omit maps using the program *TOM*, a derivative of *FRODO* (Jones, 1985). A complete set of omit maps

Table 1. *Amino-acid substitutions between salivary and pancreatic amylases*

Those residues that differ in charge are indicated in bold. Overall, salivary amylase has a net negative charge compared to pancreatic amylase.

Residue position	Salivary amylase	Pancreatic amylase	Domain
4	Ser	Pro	*A*
52	His	Tyr	*A*
163	Ser	Thr	*B*
171	Gly	**Glu**	*A*
196	Ile	Leu	*A*
224	**Glu**	Ala	*A*
287	Met	Val	*A*
347	Tyr	Gln	*A*
349	**Glu**	Gln	*A*
352	**Lys**	Asn	*A*
363	**Asp**	Asn	*A*
367	Thr	Ile	*A*
396	Asn	Ile	*A*
435	Thr	Ser	*C*

in which ten residues were successively left out over the entire course of the polypeptide chain were also examined and further adjustments made as necessary. Water molecules were selected when they appeared as a peak that was at least 3–4σ greater than the standard deviation of the map and less than 3.2 Å away from a hydrogen-bond acceptor or donor. Further refinement utilized a restrained-parameter least-squares refinement as implemented in the program *PROLSQ* (Hendrickson, 1985) with simultaneous refinement of the positional and temperature-factor parameters of the model atoms.

The resolution of the refinement was extended from 2.5 to 1.6 Å in stages (2.5, 2.2, 2.0, 1.8 and 1.6 Å) interspersed by manual fittings of the model to sequential omit maps covering the entire course of the polypeptide chain. In the final two stages, omit maps were also calculated that excluded water molecules and all associated atoms within a sphere of 6.0 Å as an additional check of the significance of these groups. Additional water molecules were selected using the ASIR search method (Tong *et al.*, 1994) and included in refinement only when their thermal factors were less than 60 Å^2. While the primary sequence for salivary amylase has been previously deduced from the cDNA (Nishide *et al.*, 1986), recent nucleotide-sequence data obtained for salivary amylase during these studies (unpublished results) showed that the amino acid encoded at position 128 corresponded to Ala rather than Val. Careful examination of the density around this residue in $[F_o - F_c]$ omit maps clearly showed that a valine side chain could not be fitted into the available density. Therefore, Val128 was corrected to Ala128 in the final model. In the related human and porcine pancreatic amylases, residue 128 is an alanine. The programs *PROCHECK* (Laskowski, MacArthur, Moss & Thornton, 1992) and *X-PLOR* (Brünger, 1988) were used in the model analysis of the final structure obtained. Visualization of electron density, model building and refinement were carried out on SGI graphics systems.

Table 2. *Data-collection and refinement statistics*

Data collection	
Space group	$P2_12_12_1$
Cell parameters (Å)	
a	53.16
b	75.39
c	136.60
Resolution range (Å)	30.0–1.6
Completeness (%)	93.4
Outer shell (2.0–1.6 Å)	88.1
Inner shell (30.0–2.0 Å)	98.4
R_{sym} (%)	7.6
Refinement	
No. of reflections used	58664
Resolution range (Å)	6.0–1.6
No. of protein atoms	3946
No. of solvent molecules	170
Average thermal factors (Å^2)	
A domain	21.9
B domain	33.7
C domain	27.5
Solvent	34.8
Final refinement *R* factor (%)	18.4

Stereochemistry of refined human salivary α-amylase

Stereochemical parameter	R.m.s. deviation from ideal values	Restraint weight
Distances (Å)		
Bond (1–2)	0.010	0.020
Angle (1–3)	0.025	0.030
Plane (1–4)	0.033	0.050
Planes (Å)	0.010	0.020
Chiral volume (Å^3)	0.083	0.100
Non-bonded contacts (Å)		
Single torsion	0.210	0.300
Multiple torsion	0.171	0.300
Possible hydrogen bond	0.138	0.300
Torsion angles (°)		
Planar (0 to 180°)	2.1	3.0
Staggered (±60°, 180°)	16.3	20.0
Orthonormal (±90°)	31.1	35.0

3. Results and discussion

3.1. *Description of the structure*

The final model contains 496 amino acids, one calcium ion, one chloride ion and 170 water molecules. The *R* factor is 18.4% for 58 664 reflections ($F > 3\sigma$) in the resolution range 6.0–1.6 Å. The refinement statistics are given in Table 2. The final $2F_o - F_c$ electron-density map shows continuous density at the 1σ level for all main-chain atoms. Fig. 1 shows an electron-density map in which residues 15–17 have been superimposed to illustrate the quality of the fit of the model to the density. In general, the electron density for the chain is well defined including the N-terminal pyroglutamic acid. In the final model, the peptide bonds are essentially planar ($\langle \Delta\omega \rangle = 2.1°$).

Stereochemical parameters that describe the quality of the structure are given in Table 2. Fig. 2 provides a Luzzati (1952) plot from which the r.m.s. standard deviations in atomic positions can be estimated to be in the range of 0.20 Å. This value is generally considered to be an overestimate of the true errors in the model. A Ramachandran plot (Ramachandran & Sasisekharan, 1968) of the φ/ψ angles in the polypeptide chain is shown in Fig. 3. With few exceptions, residues fall in or near the energetically favored regions. Three residues falling into generously allowed regions are Met102, His305 and Ser414. His305 is part of a glycine-rich, highly mobile segment, while Ser414 is a potential *N*-glycosylation site. Despite repeated manual fitting of difference electron-density maps about His305 residue, φ/ψ values could not be refined to a more energetically favorable region of the Ramachandran space. The conformational angles adopted by the residues Met102 and Ser414 are discussed below.

The overall topology of salivary amylase consists of three domains: a central domain (*A*) forming a $(\beta/\alpha)_8$-barrel structure from residues 1 to 99 and 169 to 404; a long protruding loop as an excursion from domain *A* (residues 100–168) designated as domain *B*; and a C-terminal domain (*C*) consisting of 92 residues forming an all β-structure. This topology has been structurally conserved in amylases from other sources as well (Matsuura *et al.*, 1984; Buisson *et al.*, 1987; Boel *et al.*, 1990; Brady *et al.*, 1991; Swift *et al.*, 1991; Qian *et al.*, 1993; Larson *et al.*, 1994; Kadziola *et al.*, 1994; Brayer *et al.*, 1996). Fig. 4 shows the ribbon diagram of this structure.

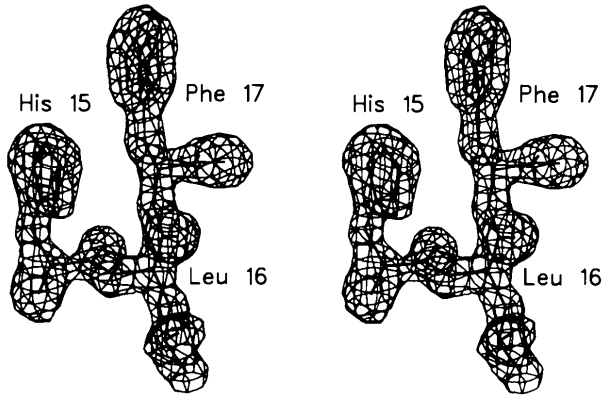

Fig. 1. A stereo diagram of an omit difference-density map in the region of residues 15–17 of the human salivary α-amylase contoured at the 4σ level. The final refined positions and bonds of the residues has been superimposed on the density and shown as dark lines.

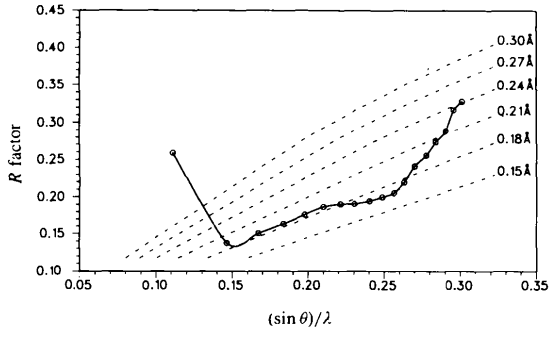

Fig. 2. A plot of the crystallographic *R* factor as a function of resolution. This analysis suggests an overall r.m.s. coordinate error for salivary amylase structure is about 0.20 Å.

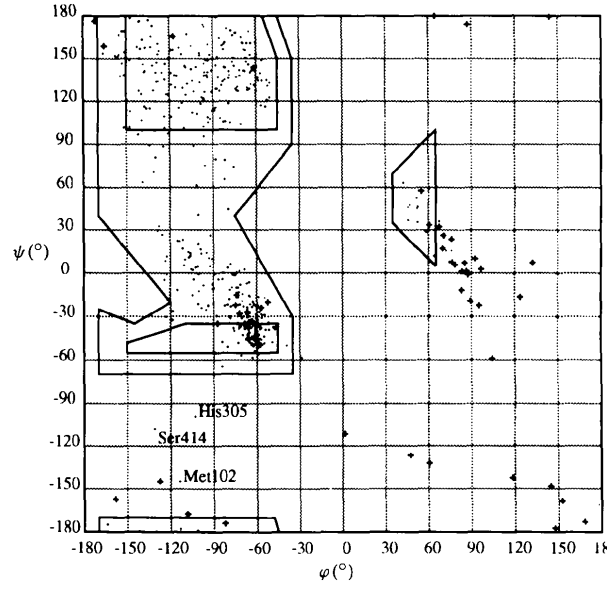

Fig. 3. Ramachandran plot for the refined model of salivary amylase. Glycine residues are shown as (+). Of the residues falling furthest from the normal limits, Met102 is strongly influenced by local interactions, the position of His305 is substantially disordered (average $B = 45$ Å^2) and Ser414 takes on a unusual conformation due to the formation of side-chain hydrogen bonds (see Fig. 9).

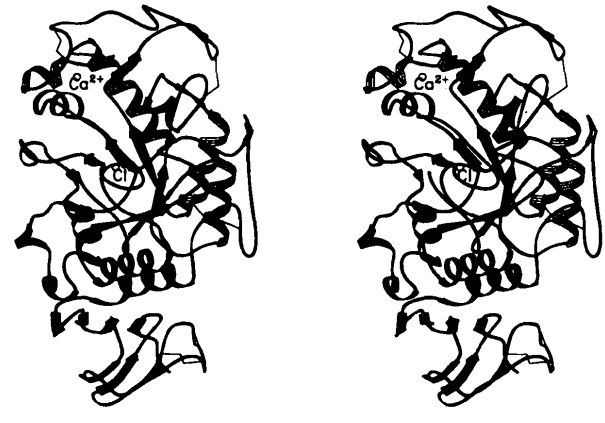

Fig. 4. Stereoview of the ribbon diagram representing the overall fold of salivary amylase. The program *DSSP* (Kabsch & Sander, 1983) was used as a guide for secondary-structural assignments. Also shown are the positions of the bound calcium and chloride ions and in thin lines the positions of the disulfide bridges.

3.2. *A domain*

Structural and biochemical studies involving small substrates and substrate-like inhibitors for amylases have shown that the cleft present in domain *A* is the site of polysaccharide binding and contains the putative catalytic sites of these enzymes (Payan, Haser, Pierrot, Frey & Astier, 1980; Matsuura *et al.*, 1984). The three catalytic residues Asp197, Glu233 and Asp300 are clustered next to each other in the central portion of the cleft. Structural comparisons among the mammalian enzymes show high conservation in the backbone positions of these residues. However, the orientation of the side chain of Asp300 in porcine pancreatic (PPA) and human salivary amylases is different (Fig. 5*a*). It is notable that in PPA complexed to acarbose (G5PPA) the side chain of Asp300 adopts a conformation similar to that of the corresponding residue in salivary amylase (Qian, Haser, Buisson, Duee & Payan, 1994). The water structure around the catalytic residues, Glu233 and Asp300, is also different in these enzymes indicating that there is considerable conformational freedom available for the side chains of these catalytic residues in the absence of substrates.

3.2.1. *Role of aromatic residues in substrate binding.*

By studying the mode of action of salivary enzyme on several modified malto-oligosaccharides, Nagamine, Omichi & Ikenaka (1988) have proposed that there are at least seven, and possibly nine binding subsites for glucose residues in the substrate-binding cleft of salivary amylase (Fig. 6*a*). There is a preference for a hydrophobic residue in subsite *S*3. Subsite *S*3, by comparison to the G5PPA, is the site harboring Trp58 and Trp59. The aromatic residues Trp58–Trp59 are part of a large substrate-binding site involving residues from the *A* and *B* domains (Fig. 6*b*). In unliganded salivary amylase, the side chain of Trp59 is localized in a conformation in which its NE1 atom does not interact with either water or protein atoms. In contrast, the NE1 atom of Trp58 has several interactions with the neighboring atoms. In the unliganded structures of human salivary amylase, as well as PPA, the main-chain carbonyl O atom of Trp59 is hydrogen bonded to a water molecule. In G5PPA, however, the side chain of Trp59 enters into hydrophobic interactions with a bound saccharide unit (Qian *et al.*, 1994). In addition, the NE1 of the Trp59 side chain, which was not involved in any interaction, is now hydrogen bonded to a water molecule while the main-chain carbonyl O atom of this residue is hydrogen bonded to the penultimate glucose moiety at the non-reducing end of acarbose (subsite *S*3). The change in conformation observed for Trp59 as a result of acarbose binding is brought about by a rotation about $\chi 1$. It has been shown that the substrate-binding cleft of amylase is able to distinguish between reducing and non-reducing ends of the substrates (Omichi, Hase & Ikenaka, 1992). One aspect of generating this asymmetric environment

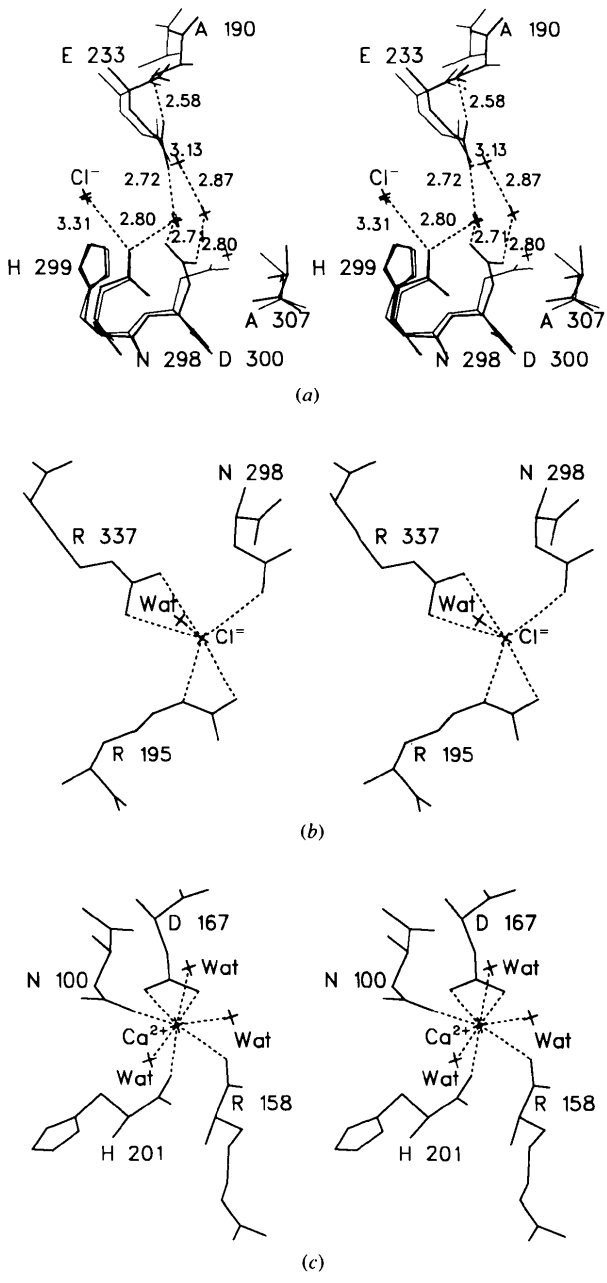

Fig. 5. The active, chloride and calcium binding sites in salivary amylase. (*a*) Stereo diagram of the superposition of the region around Glu233 and Asp300 in the active site in human salivary (dark lines) and porcine pancreatic amylase (light). Note the orientation of the Asp300 is rotated almost 90° in salivary amylase. Note also the closed network of hydrogen bonds between Asp300 and Glu233. (*b*) Stereo diagram of the coordination sphere of the chloride ion. The presence of chloride ion in the structure diminishes an otherwise close electrostatic interaction between Glu233 and Arg195. Asp96, present nearby also takes part in the reduction of electrostatic interactions in the catalytic site (see text for details). (*c*) Stereo diagram of the coordination sphere around the calcium ion. The coordination geometry is a distorted square antiprism. Note that this calcium ion is positioned in such a way to orient His201 and His101 into the active site.

may be the site occupied by Trp58 and Trp59 and its recognition of the non-reducing-end part (glycone) of the substrate by entering into hydrophobic and stacking interactions. As discussed below, another factor may involve the calcium binding site.

3.2.2. *Role of chloride in substrate binding.* The chloride ion in salivary amylase is bound by three residues (five hydrogen bonds) all of which are present in the *A* domain (Fig. 5*b*). These include the guanidinium groups of Arg195, and Arg337 and the amide side chain of Asn298 with the coordination sphere of the chloride ion being completed by a water molecule. The chloride binding site is asymmetric with respect to its binding groups in that all the ligands, including the water molecule only occupy one half of the spherical volume around the ion. The other half is occupied by Thr254, Phe256 and Phe295 which are substantially nonpolar in nature. Overall, the chloride ion is completely surrounded by protein atoms with a solvent exposure of less than 1 Å^2. In salivary amylase, Arg195 also has a salt-bridge interaction with the catalytic residue Asp197 (2.83 Å) as well as the nearby Asp96 (2.83 Å).

From a mechanistic point of view, a potential role of chloride ion could be related to the presence of a number of basic residues near the carboxyl groups of the catalytic residues and therefore, the possibility of these residues entering into unfavorable electrostatic interactions. All three acidic residues of the catalytic center (Asp197, Glu233 and Asp300) have considerable conformational freedom and interact with these basic residues to varying degrees. For example, Arg195 interacts with Asp197 (NH1···OD1 = 2.83 Å) and Glu233 (NH2···OD2 = 3.01 Å). The corresponding interactions (Arg195···Asp197 = 3.07 Å; Arg195···Glu233 = 3.43 Å) in porcine pancreatic amylase are significantly weaker (Larson *et al.*, 1994). The side-chain orientation of Asp300 of salivary amylase and its interaction with neighboring residues is strikingly similar to that observed in the G5PPA complex (Qian *et al.*, 1994) and three water molecules interact with both Asp300 and Glu233 to form a closed network of hydrogen bonds (Fig. 5*a*). In contrast, in the native PPA structure (Qian *et al.*, 1993) Asp300 and Glu233 interact with only two water molecules without forming a closed network. It is conceivable that the chloride ion plays a role in the structural organization in the nearby region to facilitate the active conformation of the enzyme by diminishing the possibility of nonproductive and unfavorable electrostatic interactions that otherwise might exist between basic and acidic residues located in the active-site region. In addition, the chloride ion may also modulate the degree of interaction between Asp197, a catalytic residue and Arg195. In this respect, Asp96 which is also located close to the chloride binding site and the active center, hydrogen bonds with Arg195 (OD1···NH1 = 2.83 Å) and may also serve to regulate the interaction between Arg195 and Asp197 as well as help orient the latter residue. It has been suggested that the chloride ion may also be instrumental in increasing the pK_a for Glu233 (Qian *et al.*, 1994). Our results and those of others clearly suggest a critical role for chloride binding in the structural and electronic organization of residues in the active site that are likely designed to facilitate substrate binding and catalysis.

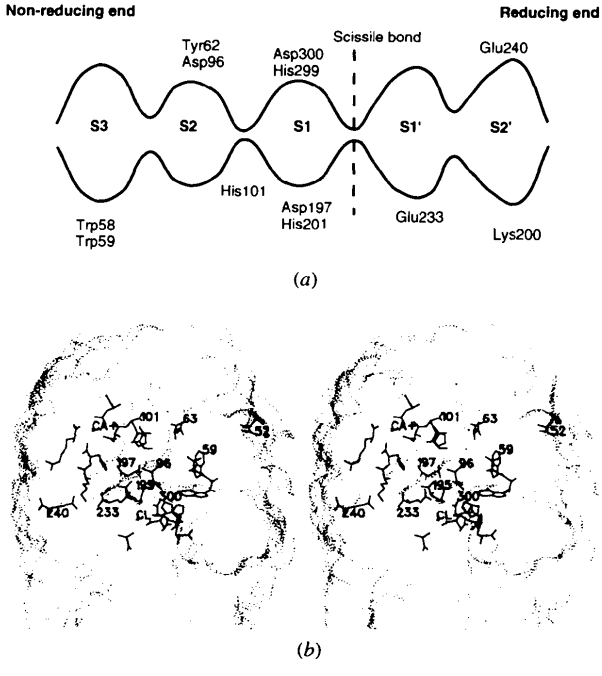

Fig. 6. (*a*) Schematic of the substrate-binding subsites in salivary amylase. (*b*) Surface representation of the substrate-binding site with the amino-acid residues involved in binding highlighted. The laying of the substrate along this cleft leads it away from the second cleft between the *A* and *C* domains. The aromatic residues, Trp58 and Trp59, are clustered near one end of the substrate-binding site and form the subsite *S3*.

3.2.3. *Salt bridges.* The helical and β-strand segments of the *A* domain generally adopt quite regular geometry. However, the helix corresponding to residues 20–33 highlights the influence salt bridges can have on the regularity of such structures (Fig. 7). The helical conformation (4→1) is broken at Tyr31 as a result of a salt bridge between Glu27 and Arg30 (OE1···NE = 2.91 Å). Glu27 is also involved in salt-bridge interactions with His386 (OE2···NE2 = 2.68 Å) and Arg387 (OE2···NE = 2.86 Å) which stabilize the interface between *A* and *C* domains. These interactions lead Tyr31 to adopt a highly distorted helical conformation ($\varphi = -89.9$; $\psi = -12.8°$). The segment continues with three additional helix-like hydrogen bonds between residues Glu27 to Leu32 (5→1), Cys28 to Ala33 (5→1) and Tyr31 to Lys35 (4→1). Residues Pro34 and Lys35 form a type I turn and link helix *Aα*1 to the β-strand *Aβ*2 of the central core region.

The segment 20–33 also contains a second salt bridge between residues Arg20 to Asp23 around which there is a noticeable bulge (Fig. 7). Domain *A* has several other salt-bridge interactions and two disulfide bridges which together help stabilize this structure. The disulfide bridge between Cys28 and Cys86 connects two helical segments ($A\alpha1$ and $A\alpha2$) of the central barrel. Both of these cysteines are located in the last turn of their respective helices. The second disulfide link between Cys378 and Cys384 is present in a 48-residue loop (341–388) connecting $A\beta8$ and $A\alpha8$.

3.2.4. *Role of residues 304–310.* The catalytic residue Asp300 is part of the most flexible loop region (residues 304–310) in human salivary amylase (Fig. 8). The role played by the loop formed by residues 304–310 in the hydrolysis of polysaccharides is apparently significant. This loop consists of four glycine, two alanine and one histidine and has the highest $\langle B \rangle$ values (Fig. 8). Because of the presence of a large number of glycine residues, this segment is highly flexible. In the presence of substrate, however, it becomes more ordered (Qian *et al.*, 1994). A cluster of glycine residues which is used as an anchor to bind adenosine triphosphate, is a characteristic of nucleotide-binding proteins (Rossmann, Moras & Olsen, 1974; Schulz, 1992). Although not conserved in all amylases, the glycine-rich segment is characteristic of mammalian amylases and is used to anchor the substrate. In the substrate-bound state, the glycine-rich sequence of mammalian amylases behaves similar to the glycine-rich sequences of nucleotide-binding proteins and protein kinases (Bossemeyer, 1995). It appears likely that this segment may be used as a gateway for substrate binding and product release by amylase. In the absence of the substrate, this loop is flexible and may adopt one of the conformations observed in either PPA or human pancreatic or salivary amylases (open position). Upon substrate binding and during hydrolysis, the segment may help in holding the substrate in place in the catalytic site (closed position). After the reaction, the products are released by the movement of the glycine-rich segment to the open position. Thus, the segment 300–310 is critical in the binding and hydrolysis of substrates.

3.3. *B domain*

The *B* domain, with no defined topology, occurs as an excursion from the TIM barrel and connects the strand $A\beta3$ to helix $A\alpha3$. This domain has a mixture of helical and extended structures and also contains the tightly bound calcium ion. The *B* domain has the only cysteine residue that is not disulfide linked (Cys103). The side-chain sulfhydryl group of this residue is completely buried. The $S\gamma$ atom of Cys103 is also weakly hydrogen bonded to the main-chain carbonyl O atom of Asn104 ($S\cdots O = 3.30$ Å). This type of hydrogen-bond ($S—H\cdots O$) interaction is very rare in globular proteins. In PPA, residue 119 (Phe119 in salivary amylase) is a cysteine and its $S\gamma$ atom is very close to the $S\gamma$ atom of Cys103 (~4.0 Å). Met102, which occurs in a generously allowed region in the Ramachandran plot (Fig. 3), is located between His101 and Cys103 and is part of the extended structure in the *B* domain (residues 101–104). The following factors may contribute to the conformational angles adopted by Met102.

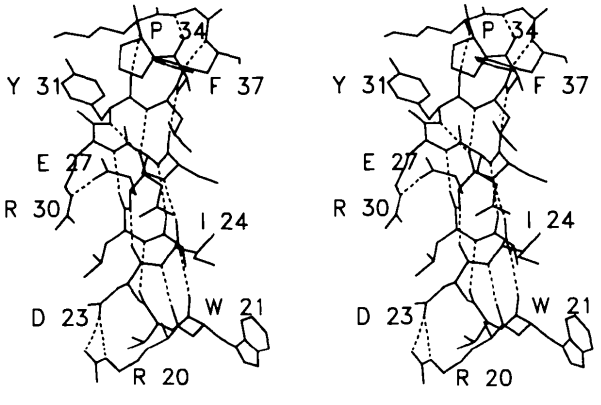

Fig. 7. Influence of two salt bridges on the regularity of helix composed of residues 20–33. The first such interaction between Glu27 and Arg30 breaks the helix at Tyr31. The second, the result of interaction between Arg20 and Asp23, creates a bulge near the N-terminus of this helical segment.

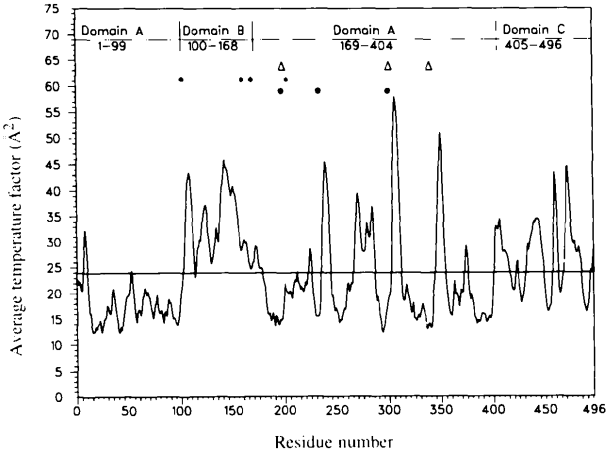

Fig. 8. A plot of the polypeptide chain mobility with the average *B* factor for each residue plotted against residue number. The average temperature factor for the main-chain atoms was 23.9 Å^2 and is represented by the horizontal line. Also shown in the plot are the location of the catalytic residues (•) and the residues involved in the binding of calcium (*) and chloride (Δ) ions. The division of the polypeptide chain into the three domains is indicated at the top of the plot. Three segments located near the substrate-binding site (residues 237–241, 304–310 and 341–350) have high thermal motion ($\langle B \rangle = 45$ Å^2). The entire *B* domain (residues 100–168) is also highly flexible. For the side-chain atoms the overall average temperature factor was 24.9 Å^2 while for the 170 water molecules included in the refinement the average *B* values was 34.8 Å^2 and ranged from 12 to 60 Å^2 (data not shown).

First, mutational studies on human pancreatic amylase in which His101 was mutated to Asn (Ishikawa, Matsui, Kobayashi, Nakatani & Honda, 1993) have shown that His101 plays an important role in catalysis. His101 is involved in a hydrogen-bond interaction with Tyr62 which in turn interacts with Asp96. As previously discussed, Asp96 plays a secondary role in the catalysis by diminishing the interaction between Asp197 and Arg195. This interaction network might restrain Met102 from adopting other more favorable φ/ψ values. Second, substitution of a phenyl ring instead of an —SH group (residue 119) in salivary amylase increases the potential for steric interactions. In fact, the Sγ atom of Cys103 is only 3.62 Å away from the phenyl ring. Thus, the conformational angles exhibited by Met102 may be a consequence of these local environmental factors.

3.3.1. *Calcium binding site.* Mammalian amylases have one essential calcium ion per molecule of amylase. The calcium-binding region does not resemble the classical calcium-binding EF-hand motif. The ligands that bind calcium are present in ordered structural segments: Asn100 and Asp167 are part of extended structures, Arg158 is located on a two-turn α-helix whereas His201 occurs in a 3_{10} helical segment. The ligands for calcium ion are: the OD1 and OD2 atoms of Asp167 (with interatomic distances of 2.35 and 2.33 Å), OD1 of Asn100 (at a distance of 2.33 Å), carbonyl O atom of Arg158 and His201 (2.34 and 2.35 Å, respectively). The average distance between the ligands and calcium is 2.33 Å suggesting a tight binding. The coordination sphere is a distorted square antiprism completed by three water molecules (Fig. 5*c*). Although the calcium ion is far from the chloride ion (~17 Å), it is still near the substrate-binding site as indicated from the study of acarbose bound PPA (Qian *et al.,* 1994). Of the residues that bind calcium, only His201 has been implicated in substrate binding and catalysis (Ishikawa *et al.,* 1993; Qian *et al.,* 1994).

3.3.2. *Role of calcium in substrate binding.* The calcium ion is tightly bound to residues located in the *A* (His201) and the *B* domains (Asn100, Arg158 and Asp167). His201, located near the subsites *S*1 and *S*2, has been shown to be essential for mammalian amylases to exert their optimum activity at neutral pH (Ishikawa *et al.,* 1993). The average *B* values for the residues in the *B* domain are higher than those of either the *A* or *C* domains suggesting a higher mobility for this domain (Fig. 8). The *B* domain is rendered partially rigid by the calcium ion, a disulfide between Cys141 and Cys160, and an interdomain disulfide bond between Cys70 of the *A* domain and Cys115 of domain *B*. The residues that ligand to the calcium ion are positioned at the beginning and end of the $\beta3\rightarrow\alpha3$ excursion. This arrangement makes the calcium ion binding site an anchor point for the overall mobility exhibited by the *B* domain and holds this domain near the substrate-binding cleft (Fig. 6*b*). In addition, the calcium binding may be instrumental in providing an asymmetric environment for the substrate such that the reducing and non-reducing ends are properly oriented. In this respect, it has been previously demonstrated that mammalian amylases are able to differentiate between the non-reducing and reducing ends of the polysaccharide (Omichi *et al.,* 1992). In fact, from the G5PPA complex (Qian *et al.,* 1994), it is clear that the substrate-binding cleft is asymmetric with respect to the orientation of the saccharide rings. All four CH_2—OH groups of the sugar units are oriented such that they face toward the calcium binding site rather than the chloride binding site. In this orientation, subsites *S*3, *S*2 and *S*1 provide a surface which is entirely made up of protein atoms and no water molecules. The laying of the substrate with the CH_2—OH groups geared toward the calcium site is conducive for loop 304–310, which occurs on the solvent side, to act as a gateway for the substrate-binding and product-release events. Thus, the calcium ion by virtue of its location stabilizes the structural integrity of the *A* and *B* domains, orients the His101 in the substrate-binding cleft and provides an asymmetric environment for substrate binding.

3.4. *C domain*

The *C* domain is made up of ten β-strands. Eight of these follow a flattened Greek-key topology (Richardson, 1981) while the remaining two are located in loops. Domain *C* is further removed from the substrate-binding site. Four strands of domain *C* ($C\beta1$, $C\beta2$, $C\beta3$ and $C\beta8$) pack against helices $A\alpha7$ and $A\alpha8$ from domain *A*. The four strands form a flat surface (approximately 10 × 19 Å) with protruding side chains. The interface region between domains *A* and *C* is rich in hydrophobic residues. At the interface, aromatic–aromatic interactions occur in patches interspersed by Met residues. The first patch is formed by Phe406, Phe419 and Trp409; the second one is formed by Phe487, Phe429 and Phe327. Overall, there is a shallow V-shaped cleft between domain *A* and domain *C* which contains His491 from the Cβ8 strand. The *C* domain has one disulfide bridge between Cys449 and Cys462 and a segment with higher *B* values (residues 455–465).

3.4.1. *Conformation of a potential glycosylation site.* The peptide segment Asn412-Gly413-Ser414 corresponds to the motif for *N*-glycosylation (NXS/T; Marshall, 1972) and is part of the *C*-domain Greek-key barrel structure. It occurs at the end of a loop connecting two strands formed by residues 406–420 (Fig. 9). The generously allowed conformation adopted by the residue Ser414 arises as a consequence of intramolecular loop interactions which form a closed network. The Asn412 side chain (OD1) interacts with the amide N atom of Ser414 and the side chain OG1 of the latter residue interacts with the OD1 of Asp432 with the network being closed by the OD2 of Asp432 interacting with the ND2 of Asn412. These interactions restrict Ser414 to

the generously allowed backbone conformation observed (Fig. 3). It is interesting to note that in human pancreatic amylase as well as in PPA, Ser414 is in a generously allowed region of Ramachandran space and has a similar conformation (Qian *et al.*, 1993; Larson *et al.*, 1994; Brayer *et al.*, 1996).

Earlier, the most probable conformation of the Asn-*X*-Ser motif was inferred from the crystal structure analysis of two peptides Boc-Asn(Me)-Ala-Ser-OMe and Boc-Asn(Me)-Pro-Ser-NHMe (Pinchion-Pesme, Aubry, Abbadi, Boussard & Marraud, 1988). Comparison of the conformation adopted by the segment Asn412-Gly413-Ser414 with that adopted by these peptides shows that the two differ significantly. In the small peptides, the Asn side chain protrudes out and is conducive for glycosylation. In contrast, the Asn412 side chain in salivary amylase is obscured by several residues rendering it incapable of accepting an oligosaccharide moiety from the dolichol intermediate. Thus, although the non-glycosylated salivary amylase contains the sequence motif for *N*-glycosylation, it does not adopt a conformation suitable for such glycosylation to occur. It should be noted that the triplet Asn-Xaa-Ser/Thr is a necessary but not sufficient condition for *N*-glycosylation. Unlike protein or nucleic acid biosynthesis, glycoprotein synthesis is not template driven; it is a co-translational process mediated by several enzymes located in discrete topological compartments within the cell. Under these circumstances, competition between protein folding and glycosylation may result in different degrees of occupancy of a given potential glycosylation site. Since the glycosylated and non-glycosylated isoforms of salivary amylase are the products of one gene (*AMY1*), and that there is only one potential glycosylation site in the sequence, the occurrence of glycosylated variant of salivary amylase must be considered to be the result of competition between the protein folding and glycosylation events.

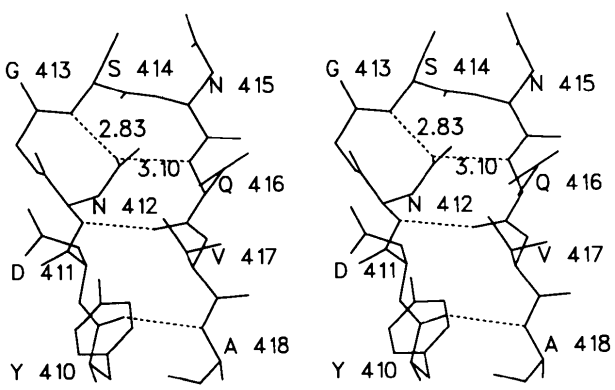

Fig. 9. The conformation of a potential *N*-glycosylation site in salivary amylase. Ser414 at the center of the site is influenced by intramolecular interactions with Asn412 and Asp432. This conformation observed is significantly different from that adopted by synthetic peptides that get glycosylated (Pinchion-Pesme *et al.*, 1988).

3.5. *Comparison of human salivary and pancreatic amylases*

Human salivary and pancreatic amylases have ~97% sequence homology. Only 14 out of the 496 residues are different between them (Table 1). Nonetheless, they exhibit significantly different behavior in several respects. First, notable differences exist between their enzymatic mode of action (Minamiura, 1988). Second, distinct monoclonal antibodies could be developed for each of these enzymes (Svens, Kapyaho, Tanner & Weber, 1989). Third, several inhibitors isolated from wheat flour show differences in their specificity toward the two amylases (O'Connor & McGeeney, 1981). Functionally, these two enzymes show little difference in their K_m for smaller substrates; however, salivary amylase has a twofold higher K_m for a heptasaccharide compared to human pancreatic amylase (Minamiura, 1988). These differences could be clarified by comparing the structures of these two enzymes. For example, the sequences of salivary amylase and human pancreatic amylase have significant substitutions in the *A* domain (Table 1). Five substitutions occur in the long loop connecting $A\beta 8$ and $A\alpha 8$ (residues 341–388). Residues Tyr347, Glu349 and Lys352 occur close to subsite 3 where the aromatic residues Trp58 and Trp59 are present. The corresponding residues in human pancreatic amylase are smaller in side-chain length (Gln347, Gln349, Asn352) and are not charged. The residues Glu349 and Lys352 (Gln and Asn in the pancreatic enzyme) would correspond to the subsite *S*4 which has been suggested to have hydrophilic residues by Nagamine *et al.* (1988). Thus, the differences in K_m values and the specificities for inhibitors between human salivary and human pancreatic amylases might arise from the polarity differences between the sequences of the long loop connecting $A\beta 8$ and $A\alpha 8$ (residues 341–388). If the residues in this loop are used to bind glucose moieties of a larger substrate such as heptasaccharides, the presence of charged residues Glu349 and Lys352 may play a role in decreasing the affinity towards human salivary amylase compared to human pancreatic amylase.

3.6. *Implication of structure on biological activity*

3.6.1. *Hydroxyapatite binding.* Salivary amylase is one of several salivary proteins that binds to hydroxyapatite (Johnsson, Levine & Nancollas, 1993). Those salivary proteins that bind more strongly to hydroxyapatite possess a high concentration of acidic residues at their N-terminus (Schlesinger & Hay, 1977; Raj, Johnsson, Levine & Nancollas, 1992; Ramasubbu, Thomas, Bhandary & Levine, 1993). Unlike these proteins, salivary amylase does not have a 'localized charge density' to bind to enamel. Nevertheless, in the three-dimensional conformation of salivary amylase the N-terminal end of the central barrel of the *A* domain, unlike the C-terminal end, adopts a flat featureless appearance. There

are several acidic residues (Asp77, Glu29, Glu369) and polar residues (Asn88 and Asn220) on this flat surface that are spatially positioned for binding to enamel or hydroxyapatite surfaces. The calcium ions on the [0001] plane of the hydroxyapatite crystal (Kay, Young & Posner, 1964) are 5.4 Å apart and are arranged in an hexagonal array. The interatomic distances between the side-chain atoms of the acidic and polar groups in salivary amylase are approximately 15–16 Å and form an isosceles triangular array. This arrangement is favorable for binding to the calcium ions on the hydroxyapatite crystal that are about 11–16 Å. Also, a larger surface area would be covered by salivary amylase. The other acidic groups on the surface of this protein are not properly positioned for efficient binding to calcium ions. Thus, it is likely that salivary amylase may possess at least one preferential surface to bind to enamel and that binding at this surface would not hinder substrate binding.

3.6.2. *Streptococcal binding.* Previously, we have shown that the histidine residues of salivary amylase play a role in its binding to oral streptococci (Scannapieco *et al.,* 1990). In these studies, histidine was modified with diethyl pyrocarbonate (DEP). At a concentration of 2 mol of DEP per mol of His in amylase, approximately four out of 12 His residues were modified to ethoxyformyl histidine. The DEP-modified amylase showed a marked reduction in both bacterial binding and enzymatic activities. The reduction in these activities diminished in the presence of maltotriose. In light of the three-dimensional structure of salivary amylase, these observations could be explained as follows. The 12 His residues occur at positions 15, 52, 101, 185, 201, 215, 299, 305, 331, 386, 476 and 491. Analysis of the solvent-accessible surface area for these histidines suggests that residues 52, 215, 305 and 476 (accessible area > 70 $Å^2$ each) might be good candidates for modification by DEP. Of these residues, His215 and His476 are located farthest from the substrate-binding sites, and may not influence the properties of salivary amylase. In contrast, His52 is almost at the glycan end of the substrate-binding site near the aromatic residues Trp58 and Trp59 (Fig. 6*b*) and His305 is in the mobile loop involved in the binding and hydrolysis of substrates. The location of His52 and His305 suggests that these may play a role in the substrate-binding activity.

Scannapieco *et al.* (1990) studied the extent of loss of bacterial binding activity and the enzymatic activity by modifying His residues in the presence and absence of maltotriose. The modification of His residues in the presence of excess maltotriose led to a greater loss of streptococcal binding activity than of catalytic activity (Scannapieco *et al.,* 1990). This result can be considered in terms of one binding site which is used by both the substrate and bacterial adhesins or two different sites, distinct from each other, one of which is used for binding bacterial adhesins and the other for binding substrates. If the bacterial binding site is the same as the enzymatic site, modification of His52 would affect bacterial binding to a greater extent than the enzymatic activity. In support of this explanation is the fact that His52 is present only in human salivary amylase and not human or porcine pancreatic amylases. Indeed, Douglas (1990) found that streptococcal binding to PPA was only 25% that of human salivary amylase while a mixture of human pancreatic and salivary amylases was 50% that of salivary amylase. Alternatively, bacteria may bind to a location far away from the substrate-binding site. Payan *et al.* (1980) suggested that a modified maltotriose (a substrate analog) binds to two sites. The first one is to the N-terminal domain of the molecule, presumably the site occupied by the acarbose moiety in the complex between acarbose and porcine pancreatic amylase (Qian *et al.,* 1994). The second site, at a more exposed surface site of the molecule, is located in the region of domain *A* facing the *C* domain near the N-terminus of *Aα*8 and is ~20 Å away from the active site (Fig. 10). In the salivary amylase structure, this site is close to His491; however, the solvent-accessible area for His491 is much lower than that of His476 which is also present in domain *C*. His491 is surrounded by Asp, Arg and Lys residues which are also present near the site occupied by acarbose (subsites *S2*, *S1* and *S1′*). The presence of multiple sites for substrate binding has been demonstrated from the study of complex between cyclodextrin and porcine pancreatic amylase also (Larson *et al.,* 1994). Whether or not one of these sites is a site for bacterial binding still remains to be seen.

3.6.3. *Role of C domain.* A lot of evidence has been accumulated over the years for the role of the *A* and *B* domains in the enzyme activity. On the other hand, the role of the *C* domain in amylases have not been addressed very well. In this regard, several possible hypotheses have been put forward. It may play an anchoring role (enabling amylase to remain seated on

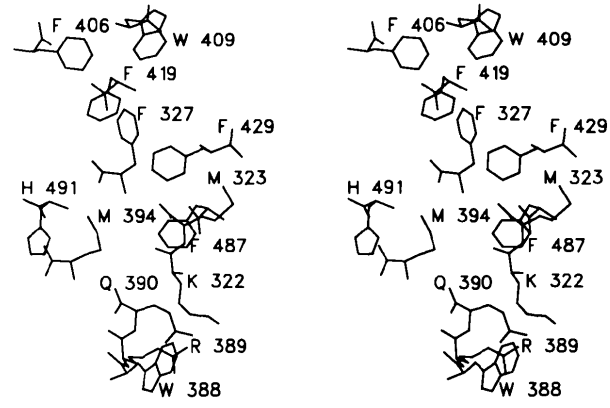

Fig. 10. The second substrate-binding site and the nearby hydrophobic patch involving aromatic and methionine groups. This site is a potential site for bacterial binding. His491 which may be involved in the bacterial binding is also shown.

the starch substrate) such that multiple attacks may occur (Robyt & French, 1970*a*,*b*; Thoma, Spradlin & Dygert, 1971) or it may have a regulatory function (O'Donnell, McGeeney & Fitzgerald, 1975). The second substrate-binding site between the *A* and *C* domains (Payan *et al.*, 1980; Buisson *et al.*, 1987) is far away from the main substrate-binding site. Bile acid salts bind only to this site (Buisson *et al.*, 1987). Therefore, the presence of separate-binding sites for substrate and bacterial adhesins in salivary amylase is well suited for the independence of the enzymatic activity and bacterial binding functions of salivary amylase. The topology of the *A* domain in barley α-amylase, which is 82 amino-acid residues shorter than salivary amylase, is essentially similar to mammalian amylases (Kadziola *et al.*, 1994). The three essential conserved regions present in the mammalian amylases are also present in barley amylase. However, this *C* domain has only five β-strands (Kadziola *et al.*, 1994). This amylase does not bind the streptococcal strains which bind to salivary amylase (Douglas, 1990).

In most of the amylases, the *C* domain appears to be loosely linked to the rest of the molecule. Of interest is the fact that there are no interdomain disulfide bridges between the *A* and *C* domains. The rigid-body mobility exhibited by the *C* domain in fungal amylases compared to mammalian amylases (Swift *et al.*, 1991; Brady *et al.*, 1991; Brayer *et al.*, 1996) is also indicative of the loose connection between the *A* and *C* domains. In light of accumulating evidence that the salivary amylase has additional roles in the oral cavity, it is tempting to suggest that the shallow cavity between the *A* and *C* domains may be the bacterial binding site. The interface is mainly defined by van der Waals contacts involving hydrophobic groups. Under suitable conditions, this interface could dissociate allowing the *C* domain to a adopt different orientation with respect to the *A* domain. It is clear that additional data are required to address the role of the *C* domain in the function of salivary amylase which is beyond the scope of this paper.* However, studies directed towards this are in progress. Recently, the streptococcal amylase-binding component has been characterized (Scannapieco, Haraszthy & Levine, 1992). The complex between this protein and salivary amylase should provide a more detailed picture of the bacterial binding and its effect on salivary amylase conformation and structure.

We thank Dr Françoise Payan for access to porcine pancreatic amylase coordinates. This work was supported by USPHS grants DE10621 and DE08240 and Medical Research Council of Canada grant MA-10940.

* Atomic coordinates and structure factors have been deposited with the Protein Data Bank, Brookhaven National Laboratory (Reference: 1SMD, R1SMDSF). Free copies may be obtained through The Managing Editor, International Union of Crystallography, 5 Abbey Square, Chester CH1 2HU, England (Reference: PT0001).

References

Alber, T., Banner, D. W., Bloomer, A. C. Petsko, G. A., Phillips, D., Rivers, P. S. & Wilson, I. A. (1981). *Philos. Trans. R. Soc. London Ser. B*, **293**, 159–171.

Al-Hashimi, I. & Levine, M. J. (1989). *Arch. Oral. Biol.* **34**, 289–295.

Banner, D. W., Bloomer, A. C., Petsko, G. A., Phillips, D. C., Pogson, C. I., Wilson, I. A., Corran, P. H., Furth, A. J., Milman, J. D., Offord, R. E., Priddle, J. D. & Waley, S. G. (1975). *Nature (London)*, **255**, 609–614.

Birkhed, D. & Skude, G. (1978). *Scand. J. Dent. Res.* **86**, 248–258.

Boel, E., Brady, L., Brzozowski, A. M., Derewenda, Z., Dodson, G. G., Jensen, V. J., Petersen, S. B., Swift, H., Thim, L. & Woldike, H. F. (1990). *Biochemistry*, **29**, 6244–6249.

Bossemeyer, D. (1995). *Trends Biochem. Sci.* **19**, 201–205.

Brady, R. L., Brozozowski, A. M., Derewenda, Z. S., Dodson, E. J. & Dodson, G. G. (1991). *Acta Cryst.* B**47**, 527–535.

Brayer, G. D., Luo, Y. & Withers, S. G. (1996). *Protein Sci.* In the press.

Brünger, A. T. (1988). *X-PLOR Manual*. New Haven: Yale University Press.

Brünger, A. T. (1990). *Acta Cryst.* A**46**, 46–57.

Buisson, G., Duee, E., Haser, R. & Payan, F. (1987). *EMBO J.* **6**, 3909–3916.

DiPaola, C., Herrera, M. S. & Mandel, I. D. (1984). *Arch. Oral Biol.* **29**, 161–163.

Douglas, C. W. I. (1990). *J. Dent. Res.* **69**, 1746–1752.

Douglas, C. W. I., Heath, J. & Gwynn, J. P. (1992). *FEMS Microbiol. Lett.* **71**, 193–197.

Douglas, C. W. I., Pease, A. A. & Whiley, R. A. (1990). *FEMS Microbiol. Lett.* **54**, 193–197.

Farber, G. K. & Petsko, G. A. (1990). *Trends Biochem. Sci.* **15**, 228–234.

Fitzgerald, P. M. D. (1988). *J. Appl. Cryst.* **21**, 273–278.

Hendrickson, W. A. (1985). *Methods Enzymol.* **115**, 252–270.

Ishikawa, K., Matsui, I., Kobayashi, S., Nakatani, H. & Honda, K. (1993). *Biochemistry*, **32**, 6259–6265.

Johnsson, M., Levine, M. J. & Nancollas, G. H. (1993). *Crit. Rev. Oral Biol. Med.* **4**, 363–370.

Jones, T. A. (1985). *Methods Enzymol.* **115**, 157–171.

Kabsch, W. & Sander, C. (1983). *Biopolymers*, **22**, 2577–2637.

Kadziola, A., Abe, J., Svensson, B. & Haser, R. (1994). *J. Mol. Biol.* **239**, 104–121.

Kay, M. I., Young, R. A. & Posner, A. S. (1964). *Nature (London)*, **204**, 1050–1052.

Klein, C. & Schulz, G. E. (1991). *J. Mol. Biol.* **217**, 737–750.

Laskowski, R. A., MacArthur, M. W., Moss, D. S. & Thornton, J. M. (1992). *PROCHECK: Programs to Check the Stereochemical Quality of Protein Structures*. Oxford Molecular Ltd, Oxford, England.

Larson, S. B., Greenwood, A., Cascio, D., Day, J. & McPherson, A. (1994). *J. Mol. Biol.* **235**, 1560–1584.

Luzzati, P. V. (1952). *Acta Cryst.* **5**, 802–810.

Marshall, R. D. (1972). *Annu. Rev. Biochem.* **41**, 673–702.

Matsuura, Y., Kusunoki, M., Harada, W. & Kakudo, M. (1984). *J. Biochem.* **95**, 697–702.

Minamiura, N. (1988). In *Handbook of Amylases and Related Enzymes*, edited by T. Yamamoto & S. Kitahata, pp. 18–22. Tokyo: Pergamon Press.

Nagamine, Y., Omichi, K. & Ikenaka, T. (1988). *J. Biochem.* **104**, 409–415.
Nishide, T., Emi, M., Nakamura, Y. & Matsubara, K. (1986). *Gene,* **28**, 263–270.
O'Connor, C. M. & McGeeney, K. F. (1981). *Biochim. Biophys. Acta,* **658**, 387–396.
O'Donnell, M. D., McGeeney, K. F. & Fitzgerald, O. (1975). *Enzymes,* **19**, 129–139.
Omichi, K., Hase, S. & Ikenaka, T. (1992). *J. Biochem.* **111**, 4–7.
Örstavik, D. & Kraus, F. W. (1973). *J. Oral Pathol.* **2**, 68–76.
Payan, F., Haser, R., Pierrot, M., Frey, M. & Astier, J. P. (1980). *Acta Cryst.* B**36**, 416–421.
Pinchion-Pesme, V., Aubry, A., Abbadi, A., Boussard, G. & Marraud, M. (1988). *Int. J. Pept. Protein Res.* **32**, 175–182.
Qian, M., Haser, R., Buisson, G., Duee, E. & Payan, F. (1994). *Biochemistry,* **33**, 6284–6294.
Qian, M., Haser, R. & Payan, F. (1993). *J. Mol. Biol.* **231**, 785–799.
Raj, P. A., Johnsson, M., Levine, M. J. & Nancollas, G. H. (1992). *J. Biol. Chem.* **267**, 5968–5976.
Ramachandran, G. N. & Sasisekharan, V. (1968). *Adv. Protein Chem.* **23**, 283–438.
Ramasubbu, N., Bhandary, K. K., Scannapieco, F. A. & Levine, M. J. (1991). *Proteins Struct. Funct. Genet.* **11**, 230–232.
Ramasubbu, N., Thomas, L. M., Bhandary, K. K. & Levine, M. J. (1993). *Crit. Rev. Oral Biol. Med.* **4**, 363–370.
Richardson, J. S. (1981). *Adv. Protein Chem.* **34**, 167–339.
Robyt, J. F. & French, D. (1970*a*). *J. Biol. Chem.* **245**, 3917–3927.
Robyt, J. F. & French, D. (1970*b*). *Arch. Biochem. Biophys.* **138**, 662–670.
Rossmann, M. G., Moras, D. & Olsen, K. W. (1974). *Nature (London),* **250**, 194–199.
Scannapieco, F. A., Bergey, E. J., Reddy, M. S. & Levine, M. J. (1989). *Infect. Immun.* **57**, 2853–2863.
Scannapieco, F. A., Bhandary, K., Ramasubbu, N. & Levine, M. J. (1990). *Biochem. Biophys. Res. Commun.* **173**, 1109–1115.
Scannapieco, F. A., Haraszthy, G. G. & Levine, M. J. (1992). *Infect. Immun.* **60**, 4726–4733.
Scannapieco, F. A., Torres, G. & Levine, M. J. (1996). In the press.
Schlesinger, D. H. & Hay, D. I. (1977). *J. Biol. Chem.* **252**, 1689–1695.
Schulz, G. E. (1992). *Curr. Opin. Struct. Biol.* **2**, 61–67.
Svens, E., Kapyaho, K., Tanner, P. & Weber, T. H. (1989). *Clin. Chem.* **35**, 662–664.
Swift, H. J., Brady, L., Derewenda, Z. S., Dodson, E. J., Dodson, G. G., Turkenburg, J. P. & Wilkinson, A. J. (1991). *Acta Cryst.* B**47**, 535–544.
Thoma, J. A., Spradlin, J. E. & Dygert, S. (1971). In *The Enzymes*, edited by P. D. Boyer, 3rd ed., Vol. 5, ch. 6, pp. 115–199. New York: Academic Press.
Tong, H., Berhuis, A. M., Chen, J., Luo, Y., Guss, J. M., Freeman, H. C. & Brayer, G. D. (1994). *J. Appl. Cryst.* **27**, 421–426.